TLR7/8-Agonist-Loaded M1-Macrophage-Derived Nanovesicles Promote the Polarization of Macrophages to Enhance Bladder Cancer Immunotherapy

Qing Zhang
Nanjing Drum Tower Hospital: Nanjing University Medical School Affiliated Nanjing Drum Tower Hospital

Tingsheng Lin
Nanjing Drum Tower Hospital: Nanjing University Medical School Affiliated Nanjing Drum Tower Hospital

Wenlong Zhang
Nanjing Drum Tower Hospital: Nanjing University Medical School Affiliated Nanjing Drum Tower Hospital

Yuanzhen Ding
Nanjing Drum Tower Hospital: Nanjing University Medical School Affiliated Nanjing Drum Tower Hospital

Xiaofeng Wang
Nanjing Drum Tower Hospital: Nanjing University Medical School Affiliated Nanjing Drum Tower Hospital

Wenfeng Lu
Nanjing Drum Tower Hospital: Nanjing University Medical School Affiliated Nanjing Drum Tower Hospital

Wenmin Cao
Nanjing Drum Tower Hospital: Nanjing University Medical School Affiliated Nanjing Drum Tower Hospital

Tingzheng Wang
Nanjing Drum Tower Hospital: Nanjing University Medical School Affiliated Nanjing Drum Tower Hospital

Wei Chen
Nanjing Drum Tower Hospital: Nanjing University Medical School Affiliated Nanjing Drum Tower Hospital

Hongqian Guo (dr.ghq@nju.edu.cn)
Nanjing University Medical School Affiliated Nanjing Drum Tower Hospital

Research

Keywords: Bladder cancer, Immunotherapy, TLR7/8, Macrophage, Nanovesicles

Posted Date: September 28th, 2021

DOI: https://doi.org/10.21203/rs.3.rs-934184/v1

Abstract

Immune checkpoint inhibitors (ICIs), such as PD-1/PD-L1 antibodies, modulate the cancer killing function of immune cells in the tumor microenvironment (TME). However, immunosuppressive M2-type tumor-associated macrophages (TAMs) are abundant in bladder cancer (BC) and able to release substances such as cytokines to promote tumor growth, evade immune cell attack and lead to tumor ICIs treatment resistance. In the present study, we utilized nanovesicles derived from M1 macrophages, which contained constituents of M1 macrophages (M1 NV), and loaded the vesicles with the TLR7/8 agonist R848, a potent driver of M1 macrophages to construct M1 NV-R848 nanovesicles. Compared with M1 NV or R848 treatment alone, M1 NV-R848 was able to induce polarization of M2 macrophages into M1 macrophages more efficient both *in vitro* and *in vivo*. Intravenous injection of M1 NV-R848 improved the immunosuppressive TME and inhibited tumor growth and no significantly toxic or immunogenic in MB-49 tumor-bearing mice. In addition, compared with M1 NV-R848 treatment alone, combined injection of M1 NV-R848 and PD-L1 was able to further inhibit MB-49 tumor growth. Thus, our study demonstrates that M1 NV-R848 has the ability to promote the polarization of M2 TAMs to M1 macrophages and to enhance the efficacy of the ICIs PD-L1 in the treatment of UBC with no significantly toxic or immunogenic.

Introduction

Urothelial carcinoma of the bladder (UBC) is the 11th most common malignant tumor worldwide[1]. UBC is prone to recurrence and progression, patients need regular lifetime visits. Therefore, UBC has a significant impact on the mortality, quality of life, as well as economic burden of patients[2]. At the time of diagnosis of UBC, about 75% of cases are non-muscle invasive UBC (NMIUBC) (Ta, T1), and another about 25% of patients are muscle invasive (MIUBC) (≥ T2). For NMIUBC, the most important clinical problem is its high tumor recurrence rate and subsequent tumor progression to more severe muscle invasive UBC[3]. Surgical resection is one of the main treatments for UBC, and despite patients with surgical and systemic treatment, the prognosis of most UBC patients (especially those with muscle invasion) remains suboptimal[4].

UBC is a type of immunogenic tumor that has been treated clinically with intravesical immunotherapy using Bacillus Calmette–Guérin (BCG) in NMIBC patients for decades[5]. As shown in The Cancer Genome Atlas (TCGA), urothelial carcinoma also presents with the highest level of DNA mutations in human cancers, slightly lower than melanoma and lung cancer[6]. Immunotherapy is a therapeutic approach used to activate immune cells, such as T cells, B cells, and macrophages, to induce anticancer immune responses. Immunotherapy focuses mainly on T cell activation leading to tumor cell necrosis. The advent of immune checkpoint inhibitors (ICIs), particularly those with antibodies against programmed cell death protein 1 (PD-1) or its ligand (PD-L1) and cytotoxic T lymphocyte-associated protein 4 (CTLA-4), has improved the treatment of metastatic UBC[7, 8]. However, the main reason for the inhibition of ICI efficacy is the weakening of effector T cell activation in the immunosuppressive TME.

Tumor-associated macrophages (TAMs) are the main macrophage type involved in TME formation. TAMs are exposed to IL-4, IL-10, TGF-β1 and lactate, and polarize into M2-type macrophages in the TME[9]. M2-like TAMs have an important role in promoting tumor growth, invasion, metastasis and drug resistance[10]. Since macrophages are the main cell type interacting with cytotoxic T cells in TME, researchers have carried out relevant studies targeting macrophages for cancer immunotherapy in recent years[10-12]. Importantly, the antitumor activation of T cells by PD-L1 may be downregulated by M2 TAMs, as M2 TAMs recruit regulatory T cells and release cytokines, suppress the immune response to tumors and disrupt the destructive function of T cells[13, 14]. In contrast, classically activated M1 macrophages inhibit tumor growth by releasing proinflammatory factors, inducing stromal destruction, and normalizing the tumor vasculature[15].

Re-education strategies can not only eliminate the tumor-supporting function of TAMs, but also actively promote them to exert anti-tumor immune function and may therefore be more effective when used in combination with ICIs[16, 17]. R848, a hydrophobic imidazoquinoline-like molecule that binds to TLR-7/8, is an immunomodulator approved by the US FDA for the treatment of skin lesions and skin cancer[18]. However, the poor water solubility, unfavorable pharmacokinetics and systemic side effects make it unable to be widely used in cancer immunotherapy[19]. Recently, it was shown that R848 encapsulated in β-cyclodextrin nanoparticles promoted the delivery of R848 to TAMs *in vivo* and improved the immunotherapeutic response rate when combined with immune checkpoint inhibitor αPD-1[20]. In addition, studies have used nanovesicles from M1 macrophages (M1 NV) to repolarize M2 macrophages into M1 macrophages, which release proinflammatory cytokines and induce antitumor immune responses, enhancing the anticancer efficacy of aPD-L1[21].

In the present study, we utilized M1 NV as a drug delivery vector carrying TLR7/8-agonist R848, thus constructing novel nanoparticles (M1 NV-R848). M1 NV-R848, which contains an intracellular component of M1 macrophages and carries TLR7/8-agonist R848, has the effect of inducing repolarization of M2-like TAMs to M1-like TAMs. Our findings show that M1 NV-R848 is able to reside in UBC for a longer period of time with UBC targeting. In addition, M1 NV-R848 strongly promoted the polarization of TAM into M1 macrophages in UBC and increased $CD8^+$ T cell infiltration, thereby achieving enhanced anti-tumor efficacy of PD-L1 *in vivo* (Scheme 1).

Methods

Cell Culture: The macrophage cell line RAW264.7 and the bladder cancer cell line MB-49 were purchased from the American Type Culture Collection (Rockville, MD, USA). RAW264.7 cells were cultured in DMEM, MB-49 cells were cultured in RPMI-1640 (Invitrogen, Carlsbad, CA, USA). All media supplemented with 10% fetal bovine serum (Dainippon Pharmaceutical, Tokyo, Japan), at 37 °C in a humidified 5% CO2 atmosphere. M1 macrophages were induced by the addition of 100 ng/mL lipopolysaccharide (LPS) and 20 ng/ml IFN-γ. M2 macrophages were induced by the addition of 20 ng/mL IL-4 (Invitrogen, CA, USA).

Preparation of M0 NV, M1 NV and M1 NV-R848: To obtain M0 NV or M1 NV, we suspended RAW264.7 cells (M0 macrophages) or LPS/IFN-γ-treated RAW264.7 cells (M1 macrophages) in PBS at a concentration of 5×10^6 cells/mL. Nanometer-sized extracellular vesicles were obtained by successively extruding 11 times through polycarbonate membrane filters (Whatman) with pore sizes of 1 μm, 400 nm, and 200 nm using a microextruder (AvantiPolarLipids). The extracellular vesicles were then ultracentrifuged at 100,000 g for 2 h at 4 °C in a density gradient formed by 10 and 50% OptiPrep layers, and the extracellular vesicles obtained from the interface of the layers were further ultracentrifuged at 100,000 g for 2 h at 4 °C to obtain M0 NV or M1 NV. To obtain M1 NV-R848, 10 mg M1 NV (10 mL in PBS) was incubated with 4 mg R848 (1 mL in DMSO) (R848 purchased from DC Chemicals, Shanghai, China) and mixed for 12 h at 37 °C on a rotator. Unencapsulated R848 was removed and M1 NV-R848 was concentrated using a 30 kDa centrifugal filter. The collected M1 NV-R848 were rinsed by centrifugal filtration with an equal volume of PBS 3 times. The amount of free R848 that remained in the dialysis water was analyzed by high performance liquid chromatography (HPLC) to obtain the loading content (LC) and loading efficiency (LE) of M1 NV. The drug LC and LE for M1NV-R848 were calculated using the following equations: LC(%) =(total amount of R848 added - free R848)/ amount of M1NV *100%, LC(%) = (total amount of R848 added - free R848)/ total amount of R848 added *100%.

LC-MS/MS and Bioinformatics Analysis Proteins were extracted from macrophages and vesicles, then subjected to trypsin digestion and quantitative analysis. The peptides were subjected to NSI source processing and analyzed by tandem mass spectrometry (MS/MS) using Q Exactive TM Plus (Thermo Scientific) coupled online to UPLC. The MS/MS data were processed using MaxQuant with Integrated Andromeda search engine (v.1.5.2.8). To analyze these data, bubble plots and KEGG pathway-based heat maps were employed in order to better identify and visualize differentially expressed proteins and possible signaling pathways.

Characterization of M0 NV, M1 NV and M1 NV-R848: The morphology and particle size of M0 NV, M1 NV and M1 NV-R848 were measured by transmission electron microscopy (TEM) (Hitachi H-7650). The dynamic light scattering (DLS) of the M0 NV, M1 NV and M1 NV-R848 was measured using a Brookhaven apparatus (Brookhaven Instruments, USA). The colloidal stability of M1 NV-R848 was investigated in PBS and serum at 37 °C by measuring their mean diameter with DLS. The amount of R848 loaded in M1 NV was determined by the reverse-phase ultrahigh-performance liquid chromatography (UHPLC) method according previous report[22]. The percentages of release of R848 were calculated according to a formula, release percentage (%) = Mr/Mt, where Mr is the amount of released R848, and Mt is the total amount of loaded R848. Drug release kinetics of R848 from M1 NV-R848 were evaluated utilizing 20 kDa dialysis cassettes (Thermo Scientific). M1 NV-R848 were suspended in 10 mL of PBS at 37 ℃. The release system was maintained at 37 °C under shaking. The release medium was sampled with 0.5 mL each time, and UHPLC was used to determine the percentage of released R848. The sample was added back to the original release system.

mRNA Quantification of NVs and Cells: Total RNA was extracted from macrophages using 1 mL of Trizol (Qiagen Valencia, CA, USA). The total RNA concentration was determined using a NanoDrop spectrometer

(ND-2000, NanoDrop Technologies, USA). Six hundred nanograms of total RNA from each sample were reverse-transcribed into cDNAs, and SYBR green-based qRT-PCR was performed using a Step One Plus real-time PCR system (Applied Biosystems, USA) with TOPreal qPCR 2X PreMIX (Enzynomics, Finland). Cycling conditions were the following: initial denaturation at 95°C for 15 min, followed by 45 cycles at 95°C for 10 s, 60°C for 15 s, and 72°C for 30 s. All of the data were analyzed using the comparative Ct method. Three samples were analyzed per group.

***In Vitro* Cellular Uptake of NVs after Treatment with NVs:** M2 macrophages were prepared by the IL-4 treatments of RAW264.7 cells. M2 macrophages were allowed to attach to culture plates containing 10% (v/v) FBS-containing medium for 24 h. Subsequently, DiR-labeled M0 NV, M1 NV, M1 NV-R848 were added into the culture at a concentration of 50 μg/mL and incubated for 4 h. Cellular uptake of NVs was evaluated using fluorescence microscopy. Additionally, 4 h after the treatment with DiR-labeled NVs, M2 macrophages were washed with PBS and analyzed with FACS. Three samples were analyzed per group.

***In Vitro* Analyses of Macrophage Polarization:** M2 macrophages were treated with M0 NV, M1 NV, R848 and M1 NV-R848 for 24 h. Subsequently, cells were fixed with 4% paraformaldehyde for 10 min at room temperature and washed with PBS, subsequent staining was performed using primary antibodies against CD163 (Santa Cruz Biotechnology, CA, USA), the samples were then incubated in PBS containing rhodamine-conjugated secondary antibody (Jackson-Immunoresearch) for 1 h at room temperature, all samples were mounted with mounting solution containing 4 ', 6-diamidino-2-phenylindole (DAPI, VectorLaboratories, Burlingame, CA, USA) to stain nuclei and using a fluorescence microscope (Olympus, Tokyo, Japan). Moreover, qRT-PCR was performed to determine the expression of M1 (iNOS, IL-6 and TNF-α), M2-related genes (IL-10, Fizz-1 and IL-4), angiogenesis factor VEGF and metastatic factor CCL-18. To further confirm the expression of M1 marker IL-6 and M2 marker IL-4 in M2 macrophages treated with M0 NV, M1 NV, R848 and M1 NV-R848 for 24 h, cytokine secretion levels were analyzed using mouse IL-6 and IL-4 ELISA kits (R&D Systems, MN, USA) according to the manufacture instructions. Each group was repeated three times.

The establishment of orthotopic bladder cancer model: Female C57BL/6 mice (8 weeks old, weight 18-20 g) were purchased from the Model Animals Research Center, Nanjing University. All mice were used in accordance with the Institutional Animal Care Regulations and Use Committee (IACUC) of Nanjing Drum Tower Hospital, Medical School of Nanjing University. All animal experiments were approved by the Institutional Animal Care Committee of Jiangsu Province and the Ethics Committee of Nanjing Drum Tower Hospital, Medical school of Nanjing University. An orthotopic bladder cancer model was established in C57BL/6 mice with a minimally invasive method based on our previously published article[23]. Briefly, we made a longitudinal small incision (approximately 2 mm) on the skin of the lower abdomen of the mouse, found the bladder, and carefully clamped the bladder using smooth forceps. MB-49^{luc} cells were injected into the bladder wall using a 1-mL syringe, the bladder was returned to its original position, and the abdominal incision was closed. One week later, tumor growth in the bladder was monitored using an IVIS Spectrum computed tomography system (PerkinElmer, Waltham, MA, U.S.).

***In Vivo* Imaging of M1NV-R848 in orthotopic bladder cancer model:** The biodistributions of M0 NV, M1 NV and M1 NV-R848 were investigated using an IVIS Spectrum computed tomography system (PerkinElmer, Waltham, MA, U.S.) after intravenous injections of M0 NV, M1 NV and M1 NV-R848 into orthotopic bladder cancer model. Briefly, 100 μg M0 NV, M1 NV and M1 NV-R848 were labeled with DiR according to the manufacturer's instructions, suspended in 100 μL of PBS, and intravenously injected via the tail vein. At 24 h after injection, the mice were sacrificed, and NIR fluorescence images of the major organs (heart, liver, spleen, lung, and kidney) and tumor were acquired at a 748 nm excitation wavelength and a 780 nm emission wavelength. Then the relative fluorescence intensities of the organs and tumor were quantified using the software Living Image 3.1.

For organ toxicity analysis, MB-49 tumor-bearing mice were intravenously injected with 100 μL PBS or 50 μg M1 NV-R848 suspended in 100 μL of PBS at day 1, 6 and 13 days. Major organs (heart, liver, spleen, lung, and kidney) were retrieved at 20 days after the first injection and fixed with 4% paraformaldehyde in PBS. The samples were embedded in OCT compound, sectioned at a thickness of 4 μm, stained using H&E and imaged using an optical microscope.

Comparison of the macrophage polarization induction effects in M0 NV, R848, M1 NV and M1 NV-R848 *in vivo*: The orthotopic bladder cancer model was established in C57BL/6 mice. One week later, the bladder tumor was confirmed using an IVIS Spectrum computed tomography system. Mice were intravenously injected with PBS, M0 NV (5mg/kg), M1 NV (5mg/kg), R848 (0.5mg/kg) and M1 NV-R848 (M1 NV:5mg/kg, R848 0.5mg/kg) at day 0, day 3 and day 6. At day 20, tumors were surgically excised and frozen sections of tumors were collected. IHC staining for M1 and M2 markers was performed. Sections were treated with sodium citrate buffer (10 mM Sodium citrate and 0.05% Tween 20, pH 6.0) for 10 min at 85℃ for antigen retrieval after hydration. Prior to staining, the tissue sections on slides were blocked with 5% (v/v) normal goat serum (Gibco) and incubated with primary antibodies against iNOS (Abcam), and arginase 1 (Abcam) for 18 h at 4°C. The sections were washed three times with PBS and were incubated for 1 h with rhodamine-conjugated secondary antibodies. After washing with PBS, the slides were mounted with a mounting medium (VectaMount mounting medium, Vector Labs Inc., Burlingame, CA, USA). For FACS, tumor tissues were mechanically cut into small pieces and then next enzymatically digested (DMEM containing 1.5 mg/mL collagenase I, 125 units/mL hyaluronidase, 0.1 mg/mL DNAase I) to generate single-cell suspensions. Then, the single-tumor cell suspensions were incubated with antibodies for 30 min on ice followed by FACS.

M1 NV-R848 potentiate antitumor effects of PD-L1 inhibitors (aPD-L1) in orthotopic bladder cancer model: The orthotopic bladder cancer model was established in C57BL/6 mice. One week later, the bladder tumor was confirmed using an IVIS Spectrum computed tomography system. Mice were intravenously injected with PBS, aPD-L1 (5mg/kg), M1 NV-R848 (M1 NV: 5mg/kg, R848: 0.5mg/kg) and aPD-L1 (5mg/kg) combined with M1 NV-R848 (M1 NV: 5mg/kg, R848: 0.5mg/kg) at day 0, day 3 and day 6. At day 20, Tumor tissues were removed from euthanized mice and were homogenized after grinding with a scalpel. For IHC and H&E staining, tumor tissues were fixed with formaldehyde, embedded in paraffin, and sliced at a thickness of 4 μm. The sections of the tumor tissues were stained with H&E

and were examined using an optical microscope (Olympus, Tokyo, Japan). IHC staining with Ki67 was performed. Tumor tissues were enzymatically digested to generate single-cell suspensions. Then, the single-tumor cell suspensions were incubated with anti-CD8A antibody for 30 min on ice followed by FACS.

Therapeutic efficacy of NVs with or without aPD-L1 in subcutaneous xenograft model of bladder cancer: Female C57BL/6 Mice were anesthetized and MB-49 cells (5×10^6 cells in 100 μL PBS per mouse) were subcutaneously injected into a flank of the mice. The tumor volume (V) was estimated according to an ellipsoidal calculation, whereby $V=a\times b^2\times0.5$, where a is the largest and b is the smallest diameters of the tumor ellipsoid. When the tumor size reached 70 mm^3, either M0 NV (5mg/kg), M1 NV (5mg/kg), R848 (0.5mg/kg), M1 NV-R848 (M1 NV: 5mg/kg, R848: 0.5mg/kg) and anti-PD-L1 mAb (5mg/kg) (aPD-L1, BioXcell) only, or a combination of M1 NV (5mg/kg) and aPD-L1 (5mg/kg), R848 (0.5mg/kg) and aPD-L1 (5mg/kg), M1 NV-R848 (M1 NV: 5mg/kg, R848: 0.5mg/kg) and aPD-L1 (5mg/kg) were injected intravenously at day 0, day 3 and day 6. The tumor volume was determined every three days. At day 20, tumors were removed from euthanized mice, The sections of the tumor tissues were stained with H&E and were examined using an optical microscope (Olympus, Tokyo, Japan).

Statistical Analyses: Data were presented as mean ± standard deviation (SD). Statistical comparisons were performed using unpaired Student's t-test for two group comparisons, one way analysis of variance (ANOVA) for comparisons of more than three groups using Prism 6 (GraphPad software). Differences were considered statistically significant when $p<0.05$.

Results And Discussions

Characterization of M1 NVs.

M1 NVs were obtained from LPS-treated RAW264.7 cells (M1 macrophages) by serial extrusion through polycarbonate membranes with pore sizes of 1 μm, 400 nm, and 200 nm. Nanoparticle tracking analyses of M1 NVs showed a size distribution with a mean diameter of 161.8±7.1, 163.4 ±5.4, 164.3±9.1 of M0 NVs, M1 NV and M1 NV-R848, respectively. Analysis with transmission electron microscopic images showed the morphology of M0 NVs, M1 NV and M1 NV-R848 (Fig 1a). The particles concentration of M0 NVs, M1 NV and M1 NV-R848 analyzed by nanoparticle tracking (Fig 1b). We examined the stability of the M1 NVs in PBS and 10% (v/v) serum as measured by DLS (Fig 1c). The data showed no significant difference in hydrodynamic diameter over 72 h. The R848 loading content (LC) in M1 NV is 10%, and the R848 loading efficiency in M1 NV is 25%. The drug release profiles of M1 NV-R848 was showed in Fig 1d, the cumulative release of R848 reached 78.6% after 72 h, which indicated that drug release from M1 NV was a controlled-release process.

After the comparison of M0 NV, M1 NV, M0 macrophage and M1 macrophage, a total of 1058716.0 secondary spectrograms were obtained by mass spectrometry. After searching the database of protein theoretical data, the available number of secondary spectrograms was 217469, and the utilization rate of

spectrograms was 20.5%. A total of 68933.0 peptides were identified by spectrogram analysis, among which the specific peptides were 66184.0. A total of 6329.0 proteins were identified, of which 5686.0 were quantifiable (Fig 1e). The differentially expressed proteins of NVs produced from macrophages was compare between them separately (Fig 1f) and their related signaling pathway were also analyzed (Fig 1g and 1h). Based on the annotation of all identified proteins and the screening of differentially expressed proteins, we conducted enrichment analysis of the KEGG pathway for differentially expressed proteins in the comparison groups, in order to find out whether the differentially expressed proteins have a significant enrichment trend in some functional types. The p-value ($p<0.05$) obtained by Fisher's exact test showed the functional classification and pathway of the significant enrichment of differential proteins by means of bubble chart. The bubble chart showed that the enrichment distribution of M1 NV vs M0 NV differential upregulation protein in the KEGG pathway (Fig 1g). Based on the p-values of Fisher's exact test obtained by enrichment analysis, the related functions in different groups were clustered together using the hierarchical clustering method and plotted as a heatmap. The transverse heatmap represented the enrichment test results of different groups, and the longitudinal heatmap represented the differentially expressed enrichment related functions (KEGG pathway). The color blocks corresponding to the functional descriptions of differentially expressed proteins in different groups indicate the degree of enrichment (Fig 1h).

Cellular uptake of NVs and polarization of M2 macrophages to M1 macrophages induced by the NVs treatment *in vitro*.

The *in vitro* uptake capacity of M2 macrophages for NVs was determined by fluorescence image analysis. NVs were labeled with fluorescent dye (DiR) for fluorescence imaging (4h) and FACS analysis (1h). Results showed uptake of the M0 NV, M1 NV, M1 NV-R848 by M2 macrophages was not significantly different (Fig 2a and 2b). For obtain M2 macrophages, RAW264.7 were treated IL-4. A schematic of M2 macrophages that polarized to M1 macrophages after different treatments is shown in Fig 2c. Immunofluorescence staining of CD163 (M1 marker) in M2 macrophages treated with M0 NV, M1 NV, R848, or M1 NV-R848 was investigated. Our results showed M1 NV-R848 significantly increased M2 macrophages polarization to M1 macrophages compared to other treatment groups (Fig 2d and 2e). To further evaluate NVs polarize M2 macrophages into M1 macrophages, we assessed the mRNA expression changes of M1 markers (IL-6, iNOS, and TNF-α) and M2 markers (Fizz-1, IL-4, and IL-10) in M2 macrophages treated with M0 NV, M1 NV, R848, or M1 NV-R848 (Fig 2f and 2g). The data showed that the mRNA levels of M1 markers were significantly increased, while the mRNA levels of M2 markers were significantly down regulation in the M1 NV-R848 treated compared with other treatment groups. The mRNA expression of angiogenesis factor VEGF and metastatic factor CCL-18 were also significantly decreased in M2 macrophages treated with M1NV-R848 for 24 hours. In addition, polarization of M2 macrophages to M1 macrophages enhanced the secretion of proinflammatory cytokines (IL-6) and reduced the secretion of cytokines (IL-4) (Fig 2i and 2j).

In vivo imaging and biodistribution analysis of orthotopic bladder cancer model after tail vein injection of NVs.

To assess the tumor-targeting efficiency of NVs, we established an orthotopic bladder cancer model for experiments (Fig 3a). To evaluate the distribution of M1NVs-R848 in tumor-bearing mice, we intravenously injected fluorescent dye (DiR)-labeled M0 NV, M1 NV, and M1 NV-R848 as well as PBS into MB49 orthotopic bladder cancer-bearing C57BL/6 mice. Mice were then obtained for major organs (heart, liver, spleen, lung, and kidney) and bladder tumors. Our results showed that the fluorescence signal of the bladder tumor in M0 NV, M1 NV and M1 NV-R848-injected mice was high due to the ERP effect in tumor (Fig 3b and 3c). Subsequently, the histological analysis of major organs (heart, liver, lung, kidney, and spleen) showed that no apparent toxicity of M1 NV-R848 *in vivo* (Fig 3d).

Comparison of the macrophage polarization induction effects in M0 NV, R848, M1 NV and M1 NV-R848 *In vivo*.

To determine the M2 to M1 macrophages polarization of M1 NV-R848 *in vivo*, we compared the protein expression of the immunosuppressive M2 marker Arg-1 and the inflammatory M1 marker iNOS in tumor tissue treated with M0 NV, R848, M1 NV and M1 NV-R848, respectively. IHC results indicated that M1 macrophage markers (iNOS) were significantly increased in bladder tumor tissues after M1NV-R848 treatment, however the M2 marker (Arg1) were significantly decreased, suggesting increased polarization of M2 to M1 macrophages (Fig 4a, 4b, and 4c). In addition, FACS results also showed that M1 macrophages ($MHCII^+$ $CD206^-$ cells) was significant increase in bladder tumor tissues after M1 NV-R848 treatment (Fig 4d and 4e).

M1 NV-R848 potentiate antitumor effects of PD-L1 inhibitors (aPD-L1) in orthotopic bladder cancer model.

Our former part results indicated that M1 NV-R848 had a significant induction of polarization of M2 macrophages to the M1 type. Previous studies have shown that the increase of M1-type macrophages in the TME has the effect of enhancing the efficacy of ICIs therapy[24]. Previous studies demonstrated that cell-derived NVs including RAW264.7 cells are biocompatible and not significantly toxic or immunogenic since NVs can evade immune phagocytosis and complement system[25]. And, NVs originated from cells can retain the membrane topology of the cells and maintain stability in serum, could be used to enhance the drug delivery properties [26-28]. Therefore, we subsequently investigated whether M1 NV-R848 has the antitumor efficacy of enhancing the ICIs aPD-L1 in MB-49^{luc} orthotopic bladder cancer-bearing C57BL/6 mice. Seven days after establishment of the bladder orthotopic tumor model (day 0), the bladder tumor was confirmed by the animal near-infrared imaging instrument. Then mice were intravenously injected with PBS, aPD-L1, the combination of aPD-L1 and M1 NV, or the combination of aPD-L1 and M1 NV-R848. We found that M1 NV-R848 combined with aPD-L1 intravenously injection treatment group significantly inhibited the growth of bladder tumors compared with aPD-L1 and the combination of aPD-L1 and M1 NV at day 20. The antitumor effect was analyzed by histological examination of tumor tissues. H&E staining of the bladder cancer showed a decrease in tumor volume (Fig 5b and 5d). IHC analysis of tumor proliferation marker Ki67 indicated that the combination treatment with M1 NV-R848 and aPD-L1 had decreased proliferative capacity in bladder cancer (Fig 5e and 5f). In addition, FACs

results indicated that combination treatment of M1NV-R848 and aPD-L1 increased infiltration of $CD8^+$ T cells in bladder cancer (Fig 5g and 5h). The inhibitory effect of M1 NV-R848 on bladder tumor growth may result from polarization of M2-type TAMs to M1-type, thereby increasing $CD8^+$ T cell infiltration in the bladder cancer TME.

Therapeutic efficacy of M1 NV-R848 with or without aPD-L1 in subcutaneous xenograft model of bladder cancer.

To further investigated whether M1 NV-R848 could enhance the antitumor efficacy of ICIs, we establish the MB49 subcutaneous xenograft model in C57BL/6 mice. When the tumor size reached 70 mm^3 approximately (day 0), subcutaneous xenograft-bearing C57BL/6 mice were intravenously injected with either PBS, M0 NV, M1 NV, R848, M1 NV-R848, aPD-L1, aPD-L1 combination of M1 NV, aPD-L1 combination of R848 or a combination of M1 NV-R848 and aPD-L1. The combination of M1 NV-R848 and aPD-L1 treatment resulted in a significant decrease in tumor volume and tumor weight at day 20 compared with control groups (Fig 6a, 6b, 6c and 6e). However, the body weight of mice was no different between the different treatment group (Fig 6d). Moreover, H&E staining showed the tumor tissues necrosis were increased in mice intravenously injected with the combination of M1 NV-R848 and aPD-L1 (Fig 6f).

Conclusion

Our data demonstrate that M1 NV-R848 polarized immunosuppressive M2 type macrophages to antitumor M1 TAMs, which potentiated the antitumor efficacy of αPD-L1 in UBC. Intravenous injection of a combination of M1 NV-R848 and aPD-L1 into bladder cancer-bearing mice induced the repolarization of M2-like to M1-like TAMs and led to a significant suppression of tumor growth, as compared to the intravenously injection of either M1 NV-R848 or αPD-L1 alone. This study suggests that M1 NV-R848 can be used as an immune regulator in the TME to potentiate ICIs therapies for bladder cancer.

Declarations

Ethics approval

The study was approved by the Ethical Committee of Nanjing Drum Tower Hospital, Medical School of Nanjing University.

Consent for publication

Not applicable

Availability of data and materials

The datasets used and analyzed during the current study are available from the corresponding author on reasonable request.

Competing interests

The authors have declared that no competing interest exists.

Funding

This study was funded by the National Natural Science Foundation of China (82072822, 81802535, 81802532, 81772710, 81972388), China postdoctoral fund (223427), Nanjing Medical Science and technique Development Foundation (YKK 18064). This study was also supported by the Project of Invigorating Health Care through Science, Technology and Education Jiangsu Provincial Key Medical Discipline (ZDXKB2016014).

Authors' contributions

HQG, QZ, and TSL conceived and designed the experiments. WLZ, YZD, WFL, WMC, and WC participated in the experiments and drafted the manuscript. TZW, WFL, and XFW contributed to the sample collection and interpretation of the data. All authors read and approved the final manuscript.

Acknowledgements

Not applicable

References

1. Siegel RL, Miller KD, Jemal A. Cancer statistics, 2020. CA Cancer J Clin. 2020. 70(1): 7-30.
2. Richters A, KKH A, LALM K. The global burden of urinary bladder cancer: an update. World J Urol. 2020. 38(8): 1895-1904.
3. Brausi M, Witjes JA, Lamm D, et al. A review of current guidelines and best practice recommendations for the management of nonmuscle invasive bladder cancer by the International Bladder Cancer Group. J Urol. 2011. 186(6): 2158-67.
4. Kamat AM, Witjes JA, Brausi M, et al. Defining and treating the spectrum of intermediate risk nonmuscle invasive bladder cancer. J Urol. 2014. 192(2): 305-15.
5. Witjes JA, Bruins HM, Cathomas R, et al. European Association of Urology Guidelines on Muscle-invasive and Metastatic Bladder Cancer: Summary of the 2020 Guidelines. Eur Urol. 2021. 79(1): 82-104.
6. Lawrence MS, Stojanov P, Polak P, et al. Mutational heterogeneity in cancer and the search for new cancer-associated genes. Nature. 2013. 499(7457): 214-218.
7. Rey-Cárdenas M, Guerrero-Ramos F, de Liaño Lista A G, et al. Recent advances in neoadjuvant immunotherapy for urothelial bladder cancer: What to expect in the near future. Cancer Treat Rev. 2021. 93: 102142.

8. Dobosz P, Dzieciątkowski T. The Intriguing History of Cancer Immunotherapy. Front Immunol. 2019. 10: 2965.
9. Chanmee T, Ontong P, Konno K, Itano N. Tumor-associated macrophages as major players in the tumor microenvironment. Cancers (Basel). 2014. 6(3): 1670-90.
10. Shu Y, Cheng P. Targeting tumor-associated macrophages for cancer immunotherapy. Biochim Biophys Acta Rev Cancer. 2020. 1874(2): 188434.
11. Mills CD, Lenz LL, Harris RA. A Breakthrough: Macrophage-Directed Cancer Immunotherapy. Cancer Res. 2016. 76(3): 513-6.
12. Pan Y, Yu Y, Wang X, Zhang T. Tumor-Associated Macrophages in Tumor Immunity. Front Immunol. 2020. 11: 583084.
13. Zhao R, Wan Q, Wang Y, et al. M1-like TAMs are required for the efficacy of PD-L1/PD-1 blockades in gastric cancer. Oncoimmunology. 2020. 10(1): 1862520.
14. Pascual-García M, Bonfill-Teixidor E, Planas-Rigol E, et al. LIF regulates CXCL9 in tumor-associated macrophages and prevents CD8+ T cell tumor-infiltration impairing anti-PD1 therapy. Nat Commun. 2019. 10(1): 2416.
15. Zeng D, Ye Z, Wu J, et al. Macrophage correlates with immunophenotype and predicts anti-PD-L1 response of urothelial cancer. Theranostics. 2020. 10(15): 7002-7014.
16. Georgoudaki AM, Prokopec KE, Boura VF, et al. Reprogramming Tumor-Associated Macrophages by Antibody Targeting Inhibits Cancer Progression and Metastasis. Cell Rep. 2016. 15(9): 2000-11.
17. Ngiow SF, Young A. Re-education of the Tumor Microenvironment With Targeted Therapies and Immunotherapies. Front Immunol. 2020. 11: 1633.
18. Lu R, Groer C, Kleindl PA, et al. Formulation and preclinical evaluation of a toll-like receptor 7/8 agonist as an anti-tumoral immunomodulator. J Control Release. 2019. 306: 165-176.
19. Zhang H, Tang WL, Kheirolomoom A, et al. Development of thermosensitive resiquimod-loaded liposomes for enhanced cancer immunotherapy. J Control Release. 2021. 330: 1080-1094.
20. Rodell CB, Arlauckas SP, Cuccarese MF, et al. TLR7/8-agonist-loaded nanoparticles promote the polarization of tumour-associated macrophages to enhance cancer immunotherapy. Nat Biomed Eng. 2018. 2(8): 578-588.
21. Choo YW, Kang M, Kim HY, et al. M1 Macrophage-Derived Nanovesicles Potentiate the Anticancer Efficacy of Immune Checkpoint Inhibitors. ACS Nano. 2018. 12(9): 8977-8993.
22. Bahmani B, Gong H, Luk BT, et al. Intratumoral immunotherapy using platelet-cloaked nanoparticles enhances antitumor immunity in solid tumors. Nat Commun. 2021. 12(1): 1999.
23. Lin T, Yuan A, Zhao X, et al. Self-assembled tumor-targeting hyaluronic acid nanoparticles for photothermal ablation in orthotopic bladder cancer. Acta Biomater. 2017. 53: 427-438.
24. Najafi M, Hashemi GN, Farhood B, et al. Macrophage polarity in cancer: A review. J Cell Biochem. 2019. 120(3): 2756-2765.

25. Yang X, Shi G, Guo J, Wang C, He Y. Exosome-encapsulated antibiotic against intracellular infections of methicillin-resistant Staphylococcus aureus. Int J Nanomedicine. 2018. 13: 8095-8104.
26. Kooijmans SA, Vader P, van Dommelen SM, van Solinge WW, Schiffelers RM. Exosome mimetics: a novel class of drug delivery systems. Int J Nanomedicine. 2012. 7: 1525-41.
27. Luan X, Sansanaphongpricha K, Myers I, Chen H, Yuan H, Sun D. Engineering exosomes as refined biological nanoplatforms for drug delivery. Acta Pharmacol Sin. 2017. 38(6): 754-763.
28. Kim OY, Lee J, Gho YS. Extracellular vesicle mimetics: Novel alternatives to extracellular vesicle-based theranostics, drug delivery, and vaccines. Semin Cell Dev Biol. 2017. 67: 74-82.

Figures

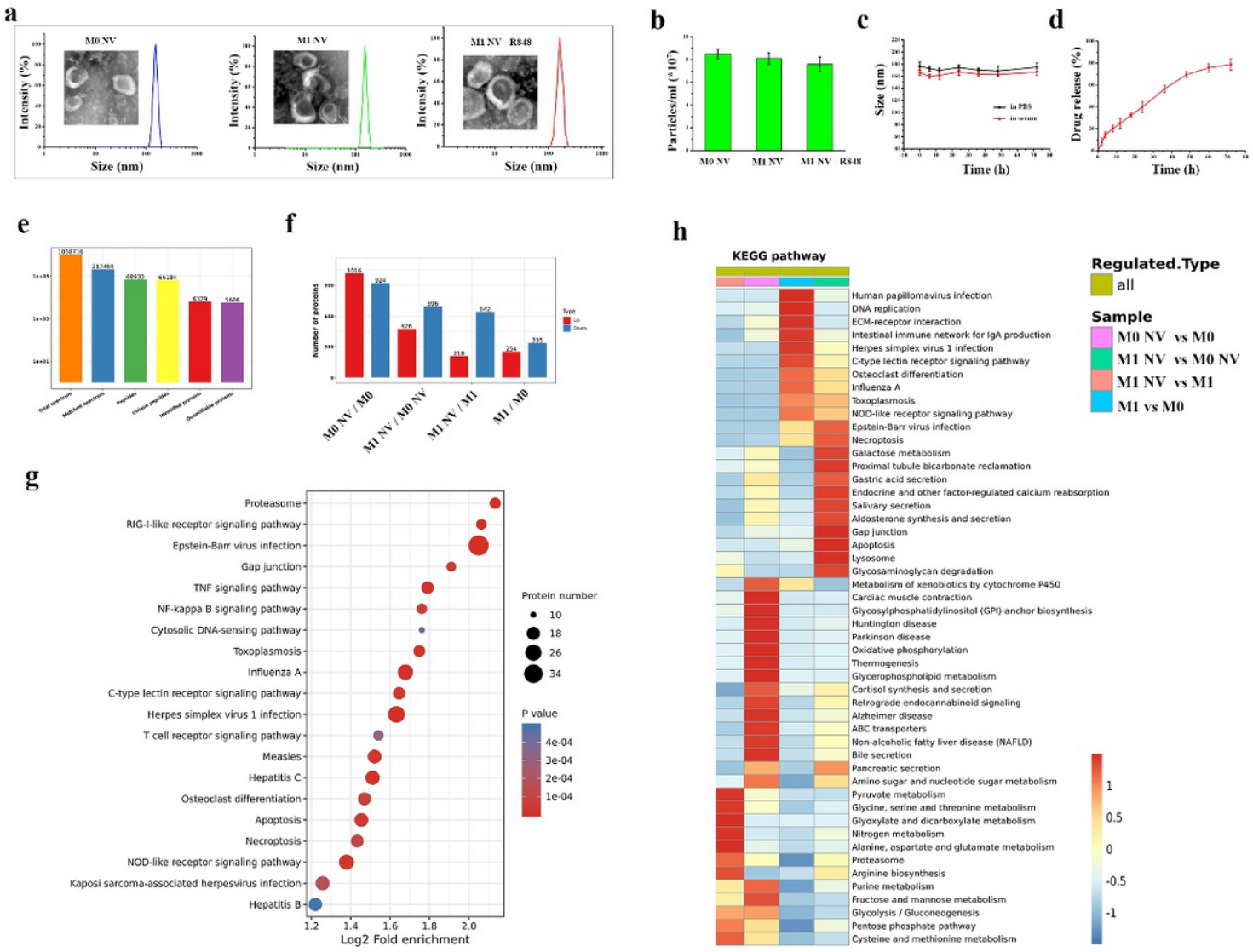

Figure 1

Characterization of NVs. (a) Size distribution and Transmission electron microscopic images of M0 NVs, M1 NV and M1 NV-R848, respectively. (b) The particles concentration of M0 NVs, M1 NV and M1 NV-

R848 analyzed by nanoparticle tracking. (c) The size profiles of M1 NV-R848 in PBS and 10% serum (v/v) over 72 h, as evaluated by DLS measurements. (d) The drug release profiles of M1 NV-R848.□e□Basic statistics of mass spectrometry data results (f) Comparison of the number of differentially expressed protein of M0 NV, M1 NV, M0 macrophage and M1 macrophage by LC-MS/MS analysis. The red bars represent the radio more than 2 while the blue bars represent the radio less than 1/2.□g□The bubble chart of differentially expressed proteins of M0, M0 NV, M1 and M1 NV which were enriched and distributed in KEGG pathway. Red represents highly significant differential proteins (P<0.01), blue indicates non-significant enrichment of GO classification. The circle size represents Fold Enrichment. (h) The heatmap of cluster analysis based on KEGG pathway enrichment analyzed of M0, M0 NV, M1 and M1 NV. The color block indicates the degree of enrichment: Red indicates the enrichment degree is strong, blue indicates the enrichment degree is weak. Data are shown as the mean ± SD.

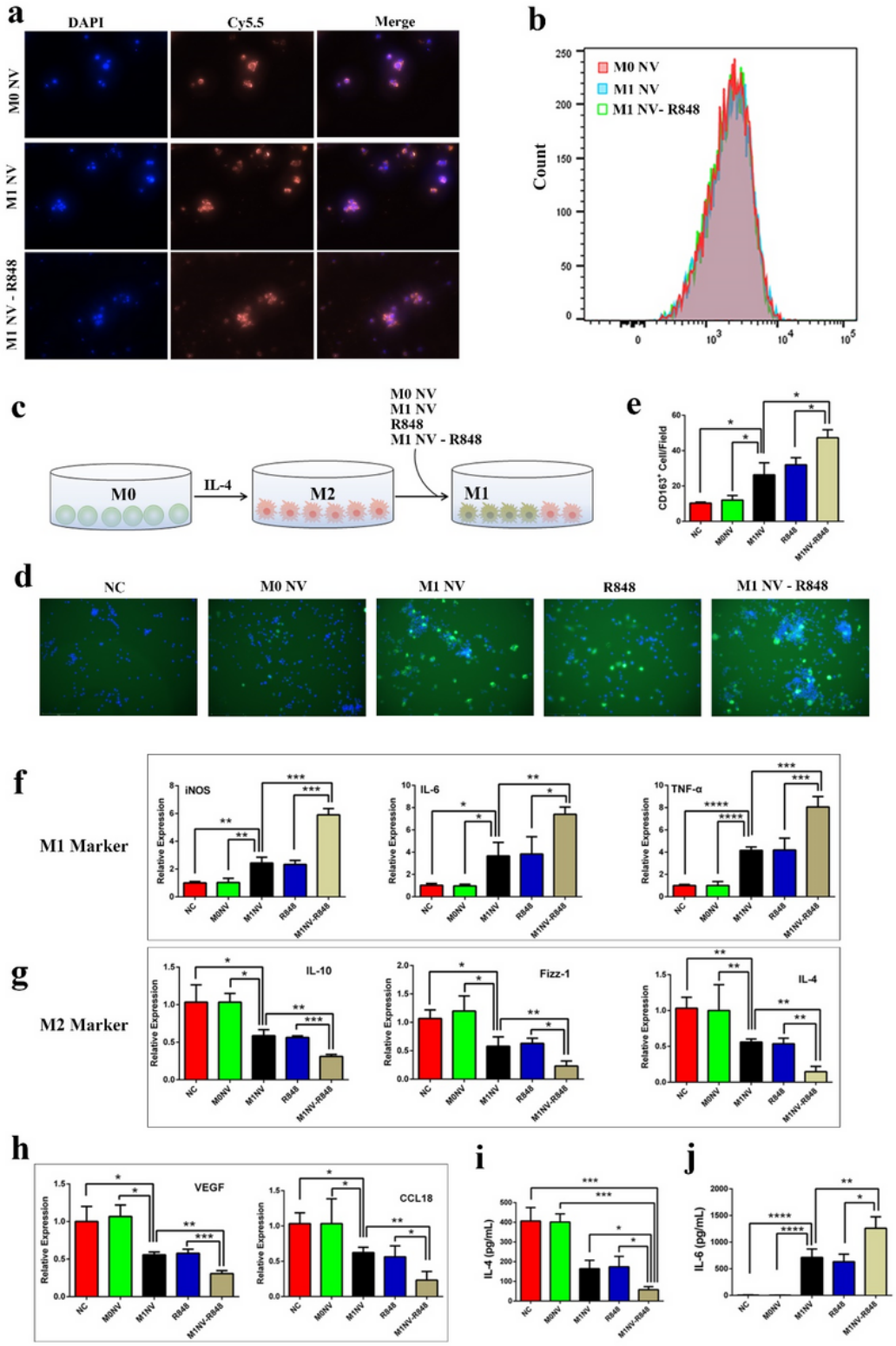

Figure 2

Cellular uptake of NVs and polarization of M2 macrophages to M1 macrophages induced by the NVs or R848 treatment in vitro. (a) Fluorescent image analysis and (b) FACS analysis for M0NV, M1NV or M1NV-R848 uptake by M2 macrophages. NVs were labeled prior to the treatments with a red fluorescent dye (DiI) for fluorescent imaging (4 h) and FACS analyses (1 h). (c) The schematic diagram of M2 macrophages polarized to M1 macrophages after different treatments. (d) Immunofluorescence staining

for CD163 (M1 marker) of M2 macrophages treated with either PBS (NC), M0 NV, M1 NV, R848 or M1 NV-R848 for 24 h. Nuclei were stained with DAPI (blue). (e) Quantification of CD163+ macrophages by immunofluorescence staining images. (f, g) Relative expressions mRNA in M1 (iNOS, IL-6, and TNF-α) and M2 macrophages (IL-10, Fizz-1 and IL-4), as evaluated by qRT-PCR. (h) The expressions of angiogenesis factor VEGF and metastatic factor CCL-18 in M2 macrophages after different treatments. (i) ELISA assay assessment for secretion of anti-inflammatory cytokine (IL-4) and pro-inflammatory cytokine (IL-6) from M2 macrophages after different treatments. Data are shown as the mean ± SD. Data are shown as the mean ± SD. *p<0.05; **p<0.01; ***p<0.001.

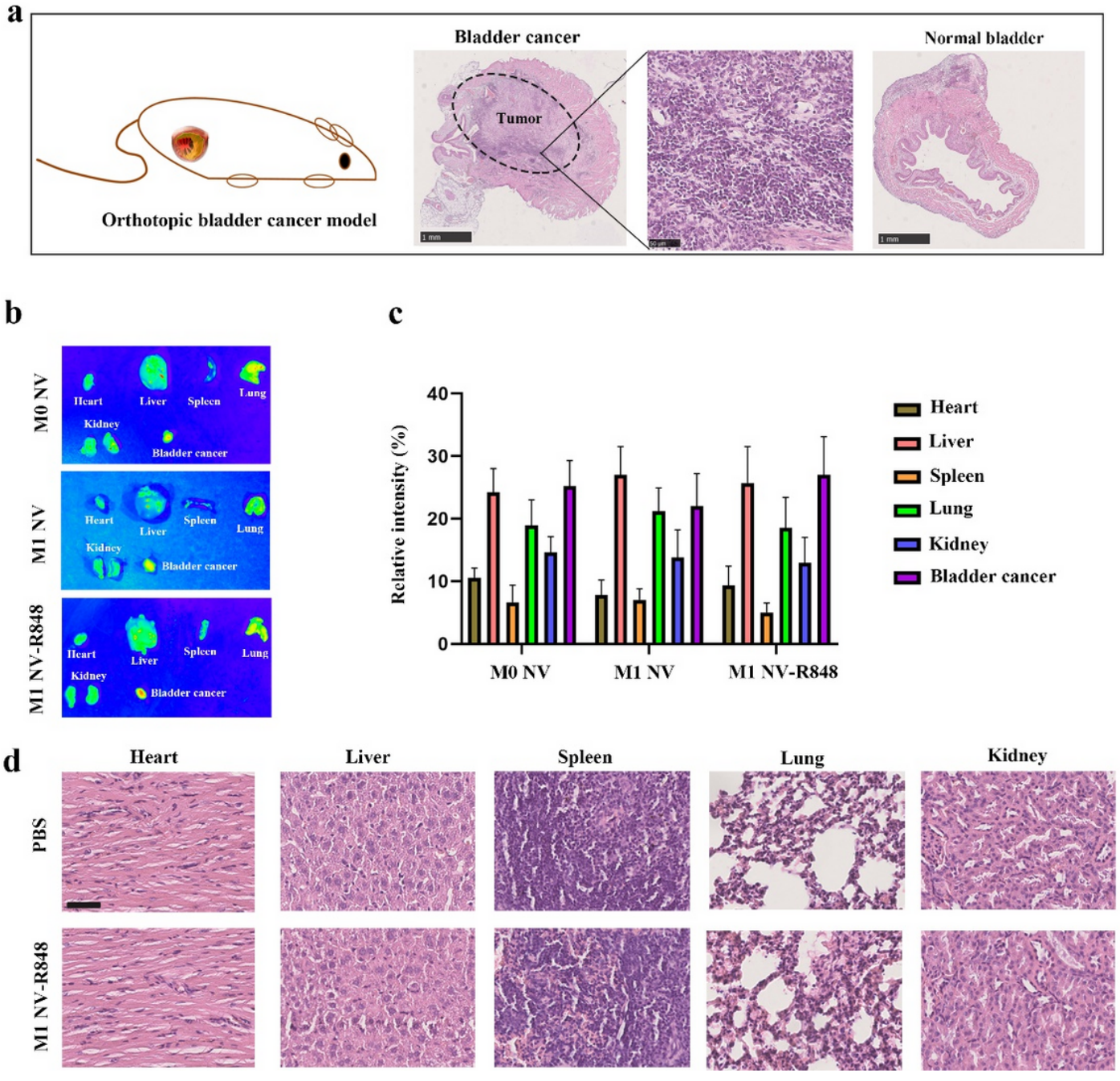

Figure 3

In vivo imaging and biodistribution analysis of orthotopic bladder cancer model after tail vein injection of NVs. (a) The HE images of orthotopic bladder cancer model and normal bladder. HE images confirmed the tumor (the dotted circle) in the bladder wall. (b) NIR fluorescence images of major organs (heart, liver, spleen, lung and kidney) and bladder bearing tumor after injection of M0 NV, M1 NV and M1 NV-R848 at 48 h. (c) Semiquantitative biodistribution of M0 NV, M1 NV and M1 NV-R848 in C57BL/6 mice determined by the averaged intensity of major organs (heart, liver, spleen, lung and kidney) and bladder bearing tumor. (d) H&E stain of the major organs (heart, liver, spleen, lung, and kidney) retrieved at 20 days after the first injection of M1 NV-R848 and PBS. Data are shown as the mean ± SD.

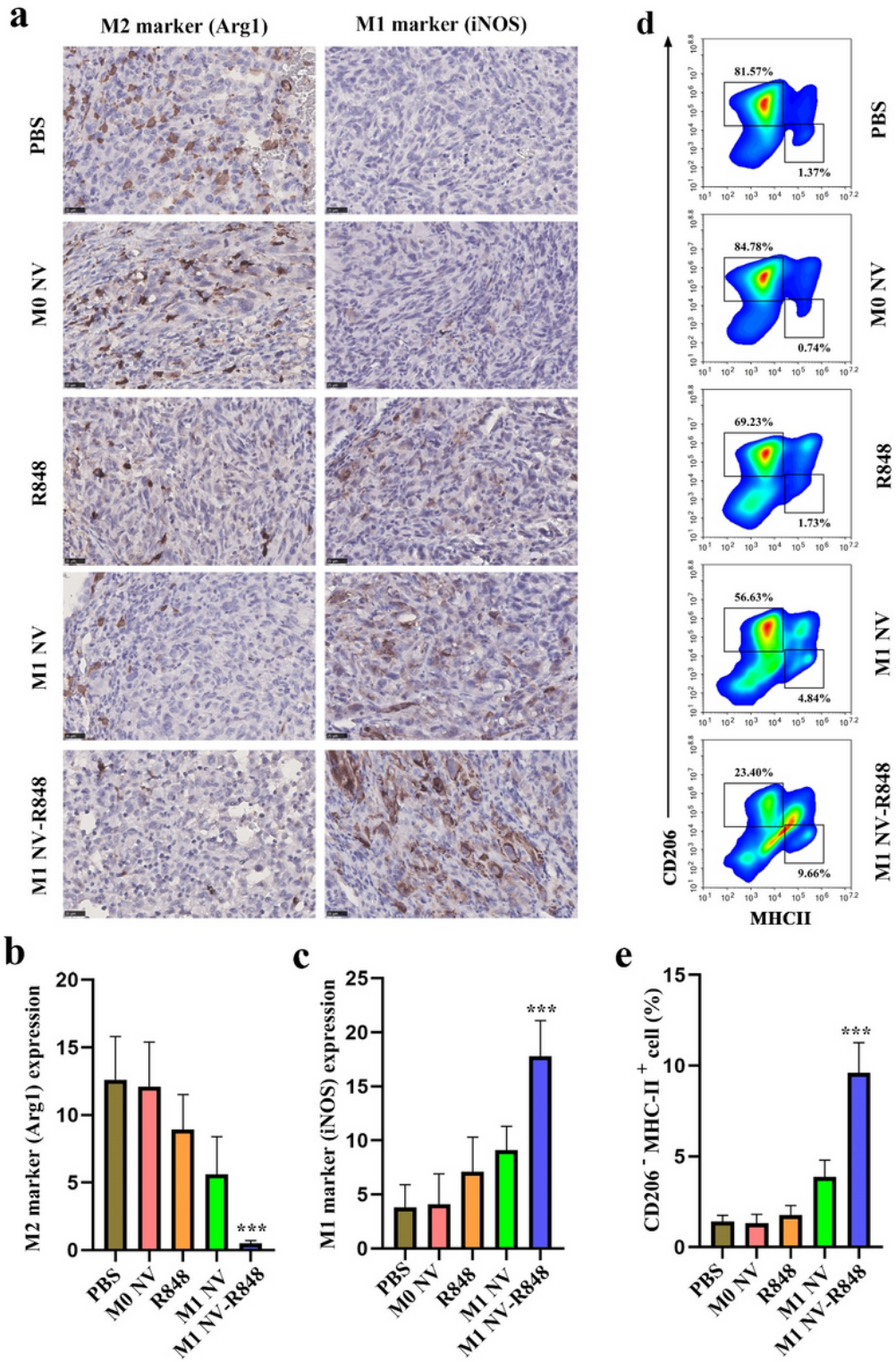

Figure 4

Comparison of the macrophage polarization induction effects in M0 NV, R848, M1 NV and M1 NV-R848 in vivo. (a) Immunohistochemical images of tissues stained with M2 marker (Arg1) and M1 marker (iNOS). (b) and (c) Quantification of Arg1 and iNOS expression in IHC staining images. (d) and (e) Flow Cytometry test the M1 marker after M1 NV-R848 treated in vivo. Data are shown as the mean ± SD. ***p<0.001.

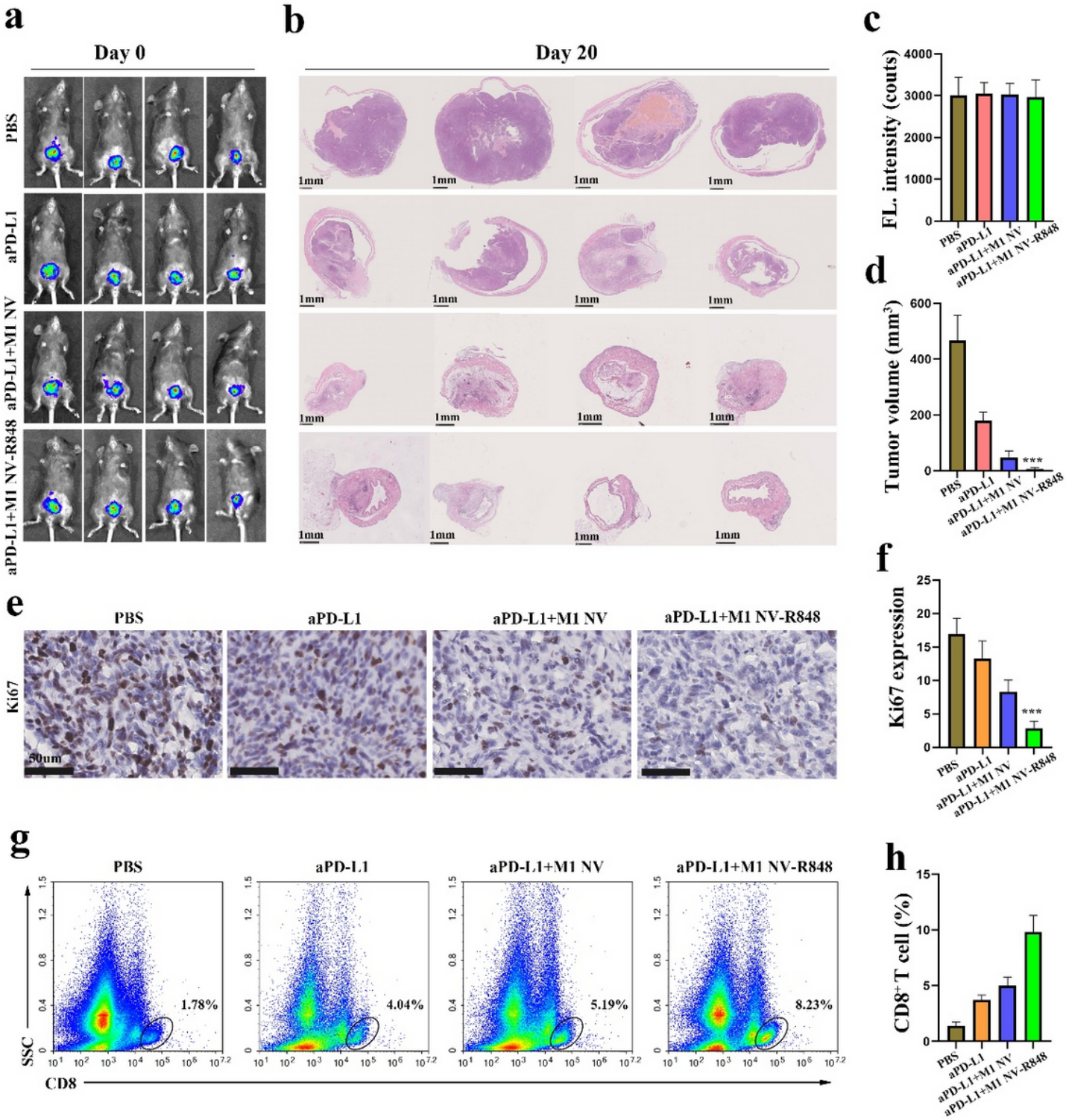

Figure 5

M1 NV-R848 potentiate antitumor effects of PD-L1 inhibitors (aPD-L1) in orthotopic bladder cancer model. (a) NIR fluorescence images of MB-49luc orthotopic bladder cancer model in different treatment at day 0. (b) The HE images of orthotopic bladder cancer model at day 20. (c) Semiquantitative analysis of MB-49luc fluorescence in bladder. (d) The bladder tumor volume in different treatment groups at day 20. (e) and (f) Ki67 expression of bladder tumor tissues in different treatment groups. (g) and (h) Flow

Cytometry test the CD8+ T cells after M1 NV-R848 treated in the UBC TME. Data are shown as the mean ± SD. ***p<0.001.

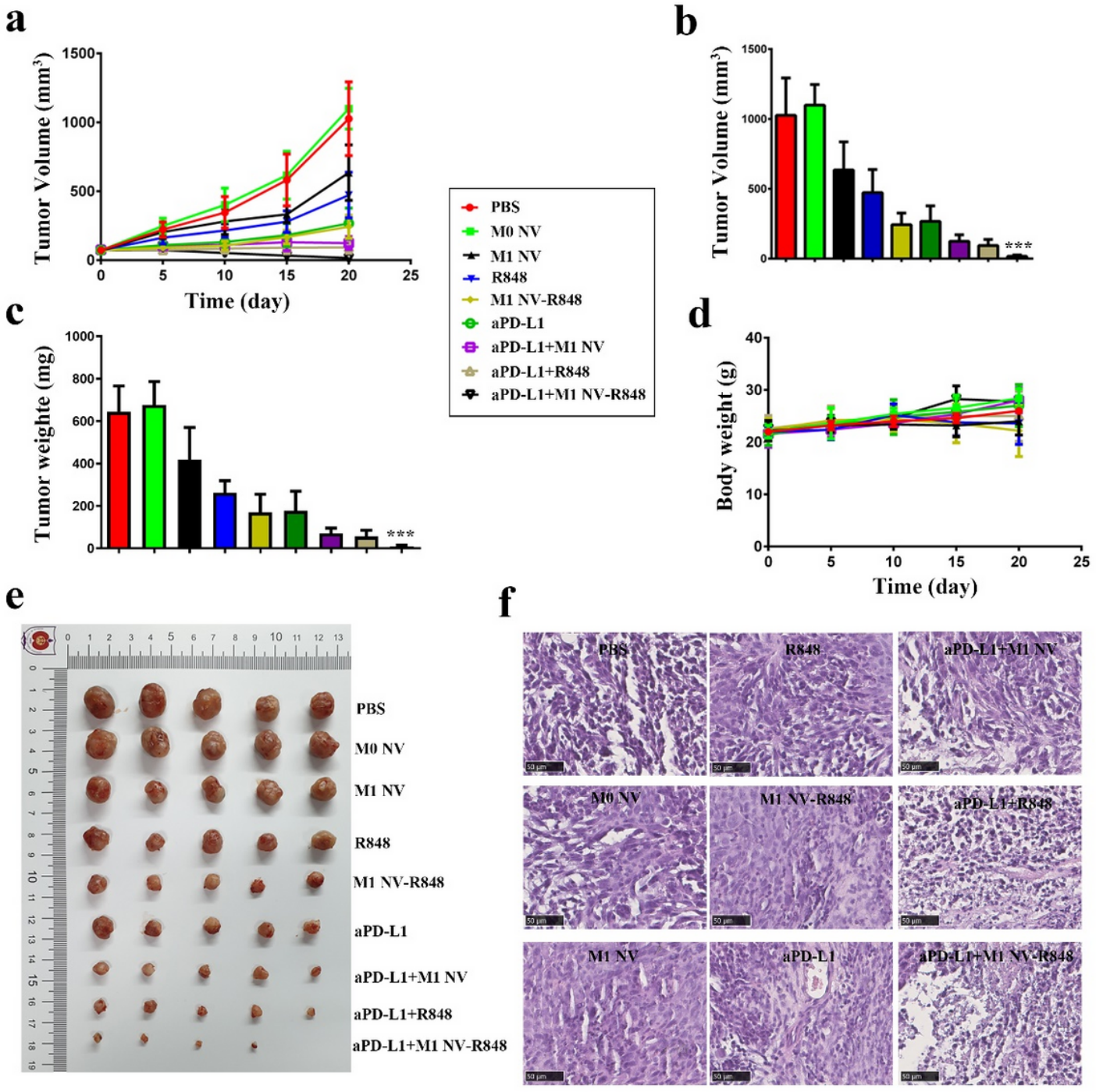

Figure 6

Therapeutic efficacy of M1 NV-R848 with or without aPD-L1 in subcutaneous xenograft model of bladder cancer. (a) Tumor growth curves after different treatments. (b) Tumor weight collected on day 20. (c) Tumor volume collected on day 20 after different treatments. (d) Body weight of mice in the different

treatments. (e) Photos of tumor masses collected on day 20. (f) H&E staining of tumor sections obtained from mice on day 20. Data are shown as the mean ± SD. *p<0.05; **p<0.01; ***p<0.001.

Supplementary Files

This is a list of supplementary files associated with this preprint. Click to download.

- schema1.png